View metadata, citation and similar papers at core.ac.uk

brought to you by CORE

provided by Kyutacar : Kyushu Institute of Technology Academic Repository

九州工業大学学術機関リポジトリ
Kyutacar
Kyushu Institute of Technology Academic Repository

Self-assembled lamellar-type nanostructure in manganite spinel (Co, Mn, Fe)3O4

著者	Horibe Y., Ishimatsu M., Takeyama S., Mori S., Kudo M., Auchi M., Tanaka M., Murakami Y.
journal or publication title	Applied Physics Letters
volume	115
number	23
page range	232401-1-232401-5
year	2019-12-02
URL	http://hdl.handle.net/10228/00007500

doi: info:doi/10.1063/1.5123780

ACCEPTED MANUSCRIPT
Applied Physics Letters
This is the author's peer reviewed, accepted manuscript. However, the online version of record will be different from this version once it has been copyedited and typeset.
PLEASE CITE THIS ARTICLE AS DOI: 10.1063/1.5123780
AIP Publishing

Self-assembled lamellar-type nanostructure in manganite spinel $(Co,Mn,Fe)_3O_4$

Y. Horibe*, M. Ishimatsu, and S. Takeyama,
Department of Materials Science & Engineering, Kyushu Institute of Technology, Kitakyushu, Fukuoka 804-8550, JAPAN

S. Mori,
Department of Materials Science, Osaka Prefecture University, Sakai, Osaka 599-8531, JAPAN

M. Kudo, and M. Auchi,
The Ultramicroscopy Research Center, Kyushu University, Fukuoka, Fukuoka 819-0395, JAPAN

M. Tanaka,
Graduate School of Engineering, Kyushu Institute of Technology, Kitakyushu, Fukuoka 804-8550, JAPAN

Y. Murakami,
The Ultramicroscopy Research Center and Department of Applied Quantum Physics and Nuclear Engineering, Kyushu University, Fukuoka, Fukuoka 819-0395, JAPAN

Keywords: lamellar nanostructure, transmission electron microscopy, electron diffraction

* Corresponding author: horibe@post.matsc.kyutech.ac.jp

Abstract

Distinct nanostructures in $(Co,Mn,Fe)_3O_4$ were investigated using X-ray diffraction techniques combined with transmission and scanning transmission electron microscopy, as well as energy dispersive X-ray spectroscopy. The size of the checkerboard nanostructure increased with annealing, followed by the appearance of lamellar nanostructures comprising different types of plate-like nanodomains because of nanoscopic spinodal decomposition of Mn and Fe

AIP Publishing
Applied Physics Letters ACCEPTED MANUSCRIPT
This is the author's peer reviewed, accepted manuscript. However, the online version of record will be different from this version once it has been copyedited and typeset.
PLEASE CITE THIS ARTICLE AS DOI: 10.1063/1.5123780

ions. Remarkable local strain relaxation at the nanoscale associated with the domain size is suggested to play an important role in the stabilization of these checkerboard and lamellar nanostructures.

Applied Physics Letters ACCEPTED MANUSCRIPT
This is the author's peer reviewed, accepted manuscript. However, the online version of record will be different from this version once it has been copyedited and typeset.
PLEASE CITE THIS ARTICLE AS DOI: 10.1063/1.5123780
AIP Publishing

Highly-anisotropic nanostructures have been engineered for applications such as high-density magnetic recording media and highly-efficient compound solar cells [1][2]. From the viewpoint of structural control and diversity of physical properties, one of the hottest and most active areas of research for these anisotropic nanostructures involves self-assembled nanomaterials that are formed by solid-state nucleation or spinodal decomposition in complex transition metal compounds [3], e. g., $BaZrO_3$ nanoparticles and/or nanorods in superconducting $YBa_2Cu_3O_{7-\delta}$ thin films [4] and ferrimagnetic $CoFe_2O_4$ nanopillars in ferroelectric $BiFeO_3$ thin film [5]. Self-assembled checkerboard nanostructures (CBNs) have also been successfully fabricated utilizing spinodal decomposition of Mn and Fe ions, where Mn-rich (Fe-poor) and Mn-poor (Fe-rich) nanodomains form as the result of the phase separation, due to the Jahn-Teller effect on octahedrally- coordinated Mn^{3+} in spinel manganites [6]-[11]. For example, CBNs with highly- anisotropic nanorods with dimensions of approximately 10 nm × 10 nm × 300 nm were found in magnetic spinel $(Co,Mn,Fe)_3O_4$ [11][12], resulting in a significant increase in coercivity [12] [13]. From theoretical studies, these self-assembled nanostructures originate from an intriguing interplay between local crystal structures and lattice strains associated with enormous Jahn-Teller distortions (~14% of the original cubic spinel structure), and the diffusion of Mn^{3+} ions in the spinel manganites [14]. Therefore, control of the lattice constants and lattice misfit strain as the result of Mn^{3+} diffusion by adjusting the annealing time and temperature can direct distinct nanostructures in these systems [15]. Furthermore, because $CoFe_2O_4$ is ferrimagnetic and $CoMn_2O_4$ is paramagnetic at room temperature, it is also tantalizing to consider the effect of configurations of magnetic and nonmagnetic nanodomains with large shape anisotropies on the magnetic properties in $(Co,Mn,Fe)_3O_4$. Herein, we report the control of nanostructures with isothermal annealing in manganese spinel oxide $(Co,Mn,Fe)_3O_4$, which can lead to drastic changes from CBNs to lamellar nanostructures

Applied Physics Letters ACCEPTED MANUSCRIPT
This is the author's peer reviewed, accepted manuscript. However, the online version of record will be different from this version once it has been copyedited and typeset.
PLEASE CITE THIS ARTICLE AS DOI: 10.1063/1.5123780
AIP Publishing

consisting of two types of tetragonal nanoplate domains and one type of cubic nanoplate domains.

$Co_{0.6}Fe_{0.9}Mn_{1.5}O_4$ polycrystalline samples used in the present study were prepared by a conventional solid state reaction in air, followed by quenching in ice water and annealing at 375 °C (in air) for 0 (as-quenched), 3.6, 10, 80, 730, and 1000 hours [9]. The samples were again quenched in ice water after annealing. Air-quenching was also tried and no significant differences were observed. The average crystal structures were measured by powder X-ray diffraction using Rigaku SmartLab at room temperature. Both crushed and Ar-ion milled samples were used for transmission electron microscopy (TEM) studies and no differences were observed. TEM observations were carried out with JEM-3000F (acceleration voltage: 300kV) and JEM-2010 (acceleration voltage: 200kV) transmission electron microscopes. Scanning transmission electron microscopy (STEM) and energy dispersive X-ray spectroscopy (EDS) were performed on ion-milled samples using a JEOL-ARM200CF STEM. The X-ray profiles and electron diffraction patterns were indexed in a consistent manner using the cubic notation based on the cubic spinel structure with the space group of $Fd\bar{3}m$.

The evolution of the nanostructures during isothermal annealing in $Co_{0.6}Fe_{0.9}Mn_{1.5}O_4$ can be seen in the powder X-ray diffraction profiles. Significant splitting of the diffraction peaks appears and increases as the annealing time increases, accompanied by obvious broadening of the peaks. Figure 1(a) shows x-ray diffraction profiles with 2 θ between 25° and 45° obtained from samples annealed at 375 °C for 0, 3.6, 10, 80, 730, and 1000 hours. Evident splittings of the fundamental Bragg reflection peaks can be seen in the X-ray diffraction profiles except for that of the 0 h- annealed sample. The most drastic changes in the profiles appear in the 10 h-annealed sample; a unique large splitting and increase of the full-width-at-half-maximum (FWHM) of the peaks are observed clearly (indicated by arrow). A further increase in annealing

Applied Physics Letters ACCEPTED MANUSCRIPT
This is the author's peer reviewed, accepted manuscript. However, the online version of record will be different from this version once it has been copyedited and typeset.
PLEASE CITE THIS ARTICLE AS DOI: 10.1063/1.5123780
AIP Publishing

time to 730 h led to a decrease of FWHM and slight changes in the 2θ position of the peaks to a lower angle, consistent with the results of a previous study [12]. Interestingly, the 1000 h-annealed sample exhibited a slight re-increase of FWHM and a shift of the diffraction peaks toward a higher angle, implying changes in the morphologies of the nanostructures associated with the diffusion of Mn ions. The 1000- h annealing also resulted in decreased magnetic coercivity, despite drastic increases from 0 h to 80 h, as reported previously [11].

In fact, the appearance of a lamellar nanostructure after significant evolution of the CBNs with annealing was found to be responsible for the characteristic features in the powder X-ray diffraction profiles. A series of bright-field images obtained from samples annealed at 375 °C for 80 h, 730 h, and 1000 h are shown in Figs. 1(b)-(d), respectively, with the corresponding electron diffraction patterns in their insets. The electron incidences are almost parallel to the [001] direction. CBNs with typical sizes of approximately 15 nm × 15 nm due to the anisotropic nanometer-scale spinodal decomposition of Mn and Fe ions was observed in the 80 h- annealed sample [Fig. 1(b)], as reported in previous studies [11] [12]. Indeed, characteristic splittings of diffraction spots in the corresponding electron diffraction pattern [inset of Fig. 1(b)] and sideview images (not shown here) indicate the presence of two types of tetragonal nanorods and two types of cubic nanorods, which are illustrated in the schematic of Fig. 1(b). As the annealing time increased, the plane-view size of checkerboard (CB) nanodomains increased, as shown in Fig. 1(c). Interestingly, our careful analysis of electron diffraction patterns revealed that the characteristic splitting of diffraction spots increased slightly with increasing size of CBN, i.e., the increased tetragonality $(a_{T(001)}-a_{T(100)})/a_{T(001)}$ from 0.11 to 0.13 and the increased relative rotation angle of the cubic unit cells by ~ 0.96°. The splitting of the $h00$ spots along the 100 direction corresponds to the tetragonality, whereas that along the 010 direction indicates the relative rotation angle of the cubic unit cells. Further prolonged annealing led to a lamellar

ACCEPTED MANUSCRIPT
Applied Physics Letters
This is the author's peer reviewed, accepted manuscript. However, the online version of record will be different from this version once it has been copyedited and typeset.
PLEASE CITE THIS ARTICLE AS DOI: 10.1063/1.5123780
AIP Publishing

nanostructure [Fig. 1(d)]. The lamellar structure consisted of band-like nanodomains approximately 100 nm wide accompanied by domain boundaries parallel or relatively rotated by 12° to each other. The corresponding electron diffraction pattern [inset of Fig. 1(d)] was completely different from that of the CBNs, reflecting the drastic changes in the nanodomains. For example, the presence of three diffraction spots split along the $[1\bar{1}0]$ direction was found around the $hh0$ reciprocal positions, whereas there was no splitting at the $h\bar{h}0$ positions, implying that the lamellar nanostructure consisted of two types of tetragonally -distorted regions and a cubic region without lattice rotation.

Dark- field imaging revealed that the lamellar nanostructure observed in the 1000 h-annealed sample originated from the regular arrangement of plate-like nanodomains with tetragonal and cubic structures, which is different from the CBNs. Figures 2(a)-(c) show the dark- field images taken using each of the split spots in the same region as in Fig. 1(d) in order to elucidate the domain configuration in the lamellar nanostructure. The insets are enlarged views near the 440 reciprocal position framed in the inset of Fig. 1(d), and the circles indicate the diffraction spot used for dark-field imaging. All the images show band-like nanodomains with alternate bright contrasts: specifically, the bright band-like nanodomains in Fig. 2(a) are parallel to each other, whereas they are inclined ~12^{o} from those observed in Fig. 2(b). In addition, the dark contrast regions in Figs. 2(a) and 2(b) become bright in Fig. 2(c). These results reveal that the lamellar nanostructure originates from the coexistence of one type of plate-like cubic nanodomain (corresponding to the diffraction spot at the original cubic reciprocal position) and two types of plate-like tetragonal nanodomains with different directions of spontaneous strain (accompanied by twin-like splitting of the diffraction spots). A tetragonal nanoplate is adjacent to the cubic nanoplates, and forms a strain- relieving domain boundary that is morphologically similar to typical twin domains. The lattice constants estimated from the

Applied Physics Letters ACCEPTED MANUSCRIPT
This is the author's peer reviewed, accepted manuscript. However, the online version of record will be different from this version once it has been copyedited and typeset.
PLEASE CITE THIS ARTICLE AS DOI: 10.1063/1.5123780
AIP Publishing

electron diffraction patterns are $a_{T(100)} \approx 8.2$ Å and $a_{T(001)} \approx 9.0$ Å for the tetragonal crystal structure, and $a_{C(100)} = a_{C(001)} \approx 8.6$ Å for the cubic structure. However, the lattice constants of the cubic and tetragonal regions estimated from sideview electron diffraction patterns (not shown here) are both $a_{T010} \approx a_{C010} \approx 8.3$ Å. Therefore, it is surprising that the unit cells in the cubic region are distorted in a somewhat tetragonal manner while those in the tetragonal region are distorted in an orthorhombic manner as a result of the nanometer-scale coexistence of two distinct phases with very different lattice constants. We will hereafter use the terms orthorhombically -distorted -tetragonal (OD-tetragonal) and tetragonally -distorted -cubic (TD-cubic) for the highly -distorted tetragonal and cubic structures, respectively. In addition, the presence of fine stripes in each band-like nanodomain suggests potential tendencies for further chemical inhomogeneities within domains, and detailed studies will be needed to elucidate the origins of these fine stripes.

Spinodal decomposition of Mn and Fe at the nanometer-scale associated with the lamellar nanostructures was directly observed in EDS analysis. Figure 2(d) shows a high-angle annular dark field STEM (HAADF-STEM) image and EDS elemental mappings of Fe (light -blue), Mn (red), and Co (yellow) obtained from the lamellar nanostructure. The evident lamellar nanostructure can be seen in the HAADF-STEM image. Note that the lamellar nanostructure was obtained from a different area of Fig. 1(d). The corresponding Fe map (lower left) and Mn map (lower right) obviously exhibit inverted contrasts resulting from the chemical inhomogeneities of Fe and Mn ions. Surprisingly, the Fe and Mn ion concentrations estimated from the EDS signal ratio were 0.2 and 2.2 in OD-tetragonal nanoplates and 1.6 and 0.8 in TD-cubic nanoplates, respectively, almost identical to the Fe and Mn ion concentrations in the CBNs (i.e., 0.2 and 2.2 in the tetragonal nanorods and 1.6 and 0.8 in the cubic nanorods), within our experimental uncertainties. In contrast, the Co ions showed no obvious tendency of phase

Applied Physics Letters ACCEPTED MANUSCRIPT
This is the author's peer reviewed, accepted manuscript. However, the online version of record will be different from this version once it has been copyedited and typeset.
PLEASE CITE THIS ARTICLE AS DOI: 10.1063/1.5123780
AIP Publishing

separation, indicating that the formation of lamellar nanostructures in this system was due to the spinodal decomposition of Fe and Mn ions at the nanometer-scale, which led to the alternate arrangement of OD-tetragonal (Mn-rich) and TD-cubic (Mn-poor) nanoplates. The spinodal decomposition in the lamellar nanostructures may have originated from the nanometer-scale spinodal decomposition related to the Jahn-Teller strain at the octahedrally coordinated Mn^{3+} ions and the relaxation of significant local strain, as suggested for the CBNs [16] [17]. Note that the Co ions occupy the tetrahedral sites in the spinel structure, whereas Mn and Fe ions mainly occupy the octahedral sites. It has been suggested an allotropic transformation takes place, which involves Mn^{3+} ions diffusing from the tetrahedral sites to the octahedral sites with annealing [12].

The lamellar nanostructures in this system exhibited distinct morphologies from the CBNs, despite the coexistence of similar OD-tetragonal and TD-cubic nanodomains with nearly identical chemical compositions. From the morphological and crystallographic features, possible schematic models for the CBN and lamellar nanostructures in this system are shown in Figs. 3. Figures 3(a) and 3(c) depict the plane-view arrangement of the OD-tetragonal and TD-cubic nanodomains, respectively, in the CBN and lamellar nanostructures, whereas Figures 3(b) and 3(d) show enlarged views in the vicinity of the boundaries framed in Figs. 3(a) and 3(c), respectively, to indicate the distortions of the unit cells near the boundary. The distortions in the OD-tetragonal unit cells in Figs. 3(b) and 3(d) are emphasized to clearly exhibit their relationships. The CBN [Fig. 3(a)] is accompanied by subtle domain configurations consisting of OD-tetragonal nanorods (α and γ, with directions of tetragonal strain perpendicular to each other) and the TD-cubic nanorods (β and δ, with the unit cells rotated by ± ~3°), which can be understood from the characteristic splitting of the diffraction spots around the $hh0$ reciprocal positions in the electron diffraction patterns [12]. In Fig. 3(b), the unit cells in the β and δ

Applied Physics Letters ACCEPTED MANUSCRIPT
This is the author's peer reviewed, accepted manuscript. However, the online version of record will be different from this version once it has been copyedited and typeset.
PLEASE CITE THIS ARTICLE AS DOI: 10.1063/1.5123780
AIP Publishing

nanorods will be rotated by ± ~3° to compensate for the profound misfit strain at the boundaries associated with very large Jahn-Teller distortions in the corner-sharing α and γ nanorods, thus stabilizing the CBN. In other words, the CBN can accommodate local lattice distortions more efficiently at the nanometer-scale than the ultrahigh-density band-like strain-relieving domains with widths on the order of several unit cells. However, the CB configuration likely becomes less efficient with the evolution of domains, and the lamellar nanostructures consisting of two types of OD-tetragonal and one type of TD-cubic domains appear with strain-relieving linear boundaries similar to twin domains. One of the remarkable features in the lamellar nanostructures is the presence of non-parallel boundaries between the two types of OD-tetragonal nanoplates of α and γ [Fig. 3(c)], in contrast to simple twin domains. As shown in Fig. 3(d), the local structure near the boundary between the OD-tetragonal and the TD-cubic domains in the lamellar nanostructure are similar to that in the CBN. The α and γ nanoplates in the lamellar nanostructure are expected to be relatively inclined at an angle of ~12° as a result of the bilateral strain-relieving linear boundaries of the TD-cubic domain, which is in excellent agreement with the angles obtained from the dark- field images. Note that all the boundaries between the TD-cubic nanoplates and the one type of tetragonal nanoplates (i.e., either one type of the α and γ nanoplates) are arranged in parallel. The lamellar structure, therefore, exhibits no relative unit-cell rotation in the TD-cubic domains, and the corresponding diffraction spots appear at the $hh0$ reciprocal positions without splitting in the electron diffraction pattern, as shown in Fig. 1(d). Consequently, the lamellar nanostructures can efficiently relieve elastic strain on a relatively large scale analogous to twin domains, whereas CBNs are preferable for gaining the total energy at small scales in this system, instead of the appearance of ultrahigh-density band-like nanodomains. Specifically, it is proposed that CBNs are more stable as the domain size decreases, whereas the lamellar nanostructure becomes dominant when the

Applied Physics Letters ACCEPTED MANUSCRIPT
This is the author's peer reviewed, accepted manuscript. However, the online version of record will be different from this version once it has been copyedited and typeset.
PLEASE CITE THIS ARTICLE AS DOI: 10.1063/1.5123780
AIP Publishing

domain size is larger.

In the $(Co,Fe,Mn)_3O_4$ system, the isothermal annealing at 375 °C for 1000 hours resulted in decreased magnetic coercivity, despite drastic increases for shorter annealing times by the presence of CBNs [11]. Because of the presence of the nanoplates, the lamellar nanostructures presumably act as less- effective pinning centers of magnetic domain walls than the CBN. As a result, the control of nanostructures is suggested to enable tuning of the coercivities in this system.

In conclusion, we investigated the formation of lamellar nanostructures in $(Co,Mn,Fe)_3O_4$ using TEM and X-ray diffraction techniques. CBN size increased with annealing, followed by the appearance of lamellar nanostructures consisting of two types of OD-tetragonal nanoplate-like domains and one type of TD-cubic nanoplate-like domains. These distinct nanoplates originated from the nanoscopic spinodal decomposition of Mn and Fe ions, similar to the CBNs in this system. The subtle balance between local lattice distortions and the misfit strain due to the coexistence of different types of nanoscopic domains with different sizes is suggested to have led to the formation of these CB and lamellar nanostructures. These results provide further insight into the nanostructure fabrication in complex transition metal compounds.

The authors would like to thank Prof. M. Ishimaru, Mr. K. Yoshidome, and Mr. H. Tabuki for their experimental support and useful discussions, and Editage (www.editage.com) for English language editing. The x-ray diffraction measurements in this study were partially performed in the Center for Instrumental Analysis, Kyushu Institute of Technology. This work was partly supported by Kyushu University Advanced Characterization Platform of the Nanotechnology Platform Japan sponsored by the Ministry of Education, Culture, Sports, Science and Technology (MEXT), Japan. This work was supported by JSPS KAKENHI,

AIP Publishing
Applied Physics Letters ACCEPTED MANUSCRIPT
This is the author's peer reviewed, accepted manuscript. However, the online version of record will be different from this version once it has been copyedited and typeset.
PLEASE CITE THIS ARTICLE AS DOI: 10.1063/1.5123780

Grant-in-Aid for Scientific Research (B) (Grant Number: 17H03393) and (C) (Grant Number: 26420681).

ACCEPTED MANUSCRIPT
Applied Physics Letters
This is the author's peer reviewed, accepted manuscript. However, the online version of record will be different from this version once it has been copyedited and typeset.
PLEASE CITE THIS ARTICLE AS DOI: 10.1063/1.5123780
AIP Publishing

References:

[1] D. J. Sellimyer, C. P. Luo, M. L. Yan, and Y. Liu, IEEE Trans. Magn. **37**, 1286–1291 (2001).

[2] P. V. Kamat, J. Phys. Chem. C **112**, 18737–18753 (2008).

[3] A. Chen, Q. Su, H. Han, E. Enriquez, and Q. Jia, Adv. Mater. **31**, 1803241 (2019).

[4] J. L. MacManus-Driscoll, S. R. Foltyn, Q. X. Jia, H. Wang, A. Serquis, L. Civale, B. Maiorov, M. E. Hawley, M. P. Maley, and D. E. Peterson, Nat. Mater. **3**, 439‑443 (2004).

[5] H. Zheng, J. Wang, S. E. Lofland, Z. Ma, L. Mohaddes-Ardabili, T. Zhao, L. Salamanca-Riba, S. R. Shinde, S. B. Ogale, F. Bai, D. Viehland, Y. Jia, D. G. Schlom, M. Wuttig, A. Roytburd, and R. Ramesh., Science **303**, 661–663 (2004).

[6] S. Yeo, Y. Horibe, S. Mori, C. M. Tseng, C. H. Chen, C. L. Zhang, and S.-W. Cheong, Appl. Phys. Lett. **89**, 233120 (2006).

[7] C. L. Zhang, S. Yeo, Y. Horibe, Y. J. Choi, S. Guha, M. Croft, S.-W. Cheong, and S. Mori, Appl. Phys. Lett. **90**, 133123 (2007).

[8] S. Park, Y. Horibe, T. Asada, L. S. Wielunski, N. Lee, P. L. Bonanno, S. M. O'Malley, A. A. Sirenko, A. Kazimirov, M. Tanimura, T. Gustafsson, and S.-W. Cheong, Nano Lett. **8**, 720–724 (2008).

[9] Y. Horibe, S. Takeyama, and S. Mori, AIP Conf. Proc. **1763**, 050005 (2016).

[10] S. M. O'Malley, P. L. Bonanno, K. H. Ahn, A. A. Sirenko, A. Kazimirov, M. Tanimura, T. Asada, S. Park, Y. Horibe, and S. -W. Cheong, Phys. Rev. **B78**, 165424 (2008).

[11] M. Ohno, S. Mori, Y. Togawa, and Y. Horibe, IOP Conf. Ser. Mater. Sci. Eng. **18**, 092052 (2011).

[12] C. L. Zhang, C. M. Tseng, C. H. Chen, S. Yeo, Y. J. Choi, and S.-W. Cheong, Appl. Phys. Lett. **91**, 233110 (2007).

[13] S Yeo, S Guha, and S. -W. Cheong, J. Phys. Condens. Matter **21**, 125402 (2009).

[14] M. Kornbluth and C. A. Marianetti, Phys. Rev. Lett. **114**, 226102 (2015).

Applied Physics Letters ACCEPTED MANUSCRIPT
This is the author's peer reviewed, accepted manuscript. However, the online version of record will be different from this version once it has been copyedited and typeset.
PLEASE CITE THIS ARTICLE AS DOI: 10.1063/1.5123780

[15] X. B. Liao, Y. Ni, H. Yang, and L. H. He, Appl. Phys. Lett. **103**, 141903 (2013).

[16] M. A. Ivanov, N. K. Tkachev, and A. Ya. Fishman, Low Temp. Phys. **25**, 459–465 (1999).

[17] M. A. Ivanov, N. K. Tkachev, and A. Ya. Fishman, Low Temp. Phys. **28**, 613–620 (2002).

ACCEPTED MANUSCRIPT
Applied Physics Letters
This is the author's peer reviewed, accepted manuscript. However, the online version of record will be different from this version once it has been copyedited and typeset.
PLEASE CITE THIS ARTICLE AS DOI: 10.1063/1.5123780
AIP Publishing

Figure Captions:

Fig. 1. (Color Online) (a) Powder X-ray diffraction patterns with 2θ between 25º and 45º obtained from $(Co,Mn,Fe)_3O_4$ samples annealed at different times. The inset displays the first quadrant of magnetic hysteresis curves with different annealing times. The results of 0 h and 80 h are referred to Ref. 11. (b), (c), and (d) Dark- field images obtained from 80, 730, and 1000 h-annealed samples, respectively. The insets correspond to selected area electron diffraction patterns with electron incidence parallel to the [001] direction. The schematic in (b) depicts a three-dimensional checkerboard nanostructure consisting of tetragonal (T) and cubic (C) nanorods.

Fig. 2. (Color Online) (a), (b), and (c) Dark-field images taken using split fundamental reflection spots around 440 reciprocal positions indicated in the insets. The arrows represent the same positions among the images. (d) HAADF-STEM images and EDS elemental mappings of Fe, Mn, and Co.

Fig. 3. (Color Online) Schematic plane-views for (a) and (b) CBNs and (c) and (d) lamellar nano-structures, along the [001] crystallographic direction. (a) and (c) represent domain configurations and (b) and (d) depicts local unit cell distortions near the domain boundaries framed in (a) and (c), respectively. Both end arrows in (a), and (c) denotes tetragonal long axis, whereas round-arrows in (a) correspond to the rotation direction of the cubic unit cell.

AIP Publishing

Applied Physics Letters ACCEPTED MANUSCRIPT

This is the author's peer reviewed, accepted manuscript. However, the online version of record will be different from this version once it has been copyedited and typeset.

PLEASE CITE THIS ARTICLE AS DOI: 10.1063/1.5123780

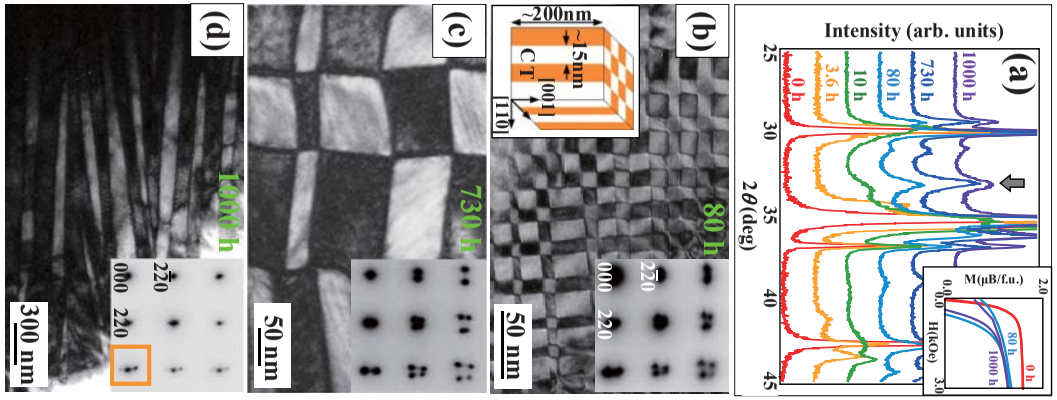

AIP Publishing

Applied Physics Letters ACCEPTED MANUSCRIPT

This is the author's peer reviewed, accepted manuscript. However, the online version of record will be different from this version once it has been copyedited and typeset.

PLEASE CITE THIS ARTICLE AS DOI: 10.1063/1.5123780

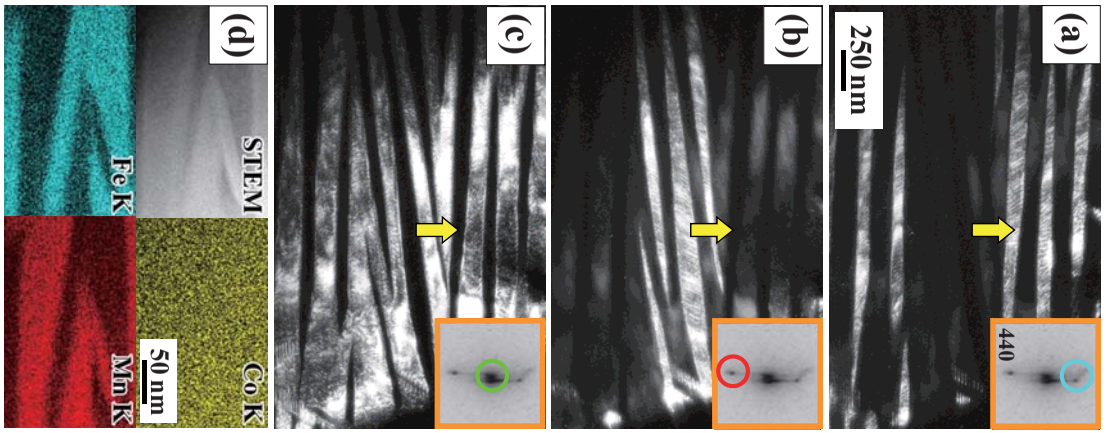

AIP Publishing

Applied Physics Letters ACCEPTED MANUSCRIPT

This is the author's peer reviewed, accepted manuscript. However, the online version of record will be different from this version once it has been copyedited and typeset.

PLEASE CITE THIS ARTICLE AS DOI: 10.1063/1.5123780